Measurement of the complex nonlinear optical response of a surface plasmon-polariton

Israel De Leon,[1,*] Zhimin Shi,[2] Andreas C. Liapis,[3] and Robert W. Boyd[1,3]

[1]*Department of Physics, University of Ottawa, Ottawa, Ontario K1N6N5, Canada*

[2]*Department of Physics, University of South Florida, Tampa, Florida 33620, USA*

[3]*The Institute of Optics, University of Rochester, Rochester, New York 14627, USA*

**Corresponding author: ideleon@uottawa.ca*

Received January 20, 2014; revised March 5, 2014; accepted March 8, 2014;
posted March 10, 2014 (Doc. ID 204475); published April 8, 2014

We observe experimentally the self-phase modulation of a surface plasmon-polariton (SPP) propagating along a gold film bounded by air in a Kretschmann–Raether configuration. Through analyzing the power dependence of the reflectance curve as a function of the incidence angle, we characterize the complex-valued nonlinear propagation coefficient of the SPP. Moreover, we present a procedure that can further extract the complex value of the third-order nonlinear susceptibility of gold from our experimental data. Our work provides direct insights into nonlinear control of SPPs utilizing the nonlinearity of metals, and serves as a practical method to measure the complex-valued third-order nonlinear susceptibility of metallic materials.

OCIS codes: (240.6680) Surface plasmons; (240.4350) Nonlinear optics at surfaces; (190.5940) Self-action effects; (190.7110) Ultrafast nonlinear optics.

http://dx.doi.org/10.1364/OL.39.002274

Surface plasmon-polaritons (SPPs) are collective charge oscillations coupled to photons at a metal–dielectric interface [1,2]. SPPs exhibit a number of properties that make them a promising nonlinear photonic platform at the nanometer scale. Such properties include the capacity for subwavelength field confinement, a strong field enhancement near the metal surface [3,4], and the fact that metals possess a strong and ultrafast third-order nonlinear response at optical wavelengths [5,6]. Because of this, substantial efforts have been devoted to the investigation of nonlinear phenomena in different plasmonic systems, such as harmonic generation and frequency mixing [7–14], self-phase modulation and plasmon–soliton formation [15–21], optically induced damping, and all-optical modulation [22–25].

In this Letter, we investigate the intensity dependence of an SPP propagating on a gold film in a Kretschmann–Raether configuration [26], and characterize experimentally for the first time its complex-valued nonlinear propagation coefficient. A measurement of this sort is of utmost importance to develop a direct understanding of how SPPs interact with themselves through the nonlinear response of the metal [17]. Furthermore, we present a procedure through which the complex-valued third-order nonlinear susceptibility of gold (Au) can be deduced accurately from the experimental data.

We consider a one-dimensional SPP waveguide consisting of a thermally evaporated Au film with a thickness of 48 ± 0.5 nm sandwiched between a glass substrate and air. Such a geometry supports an SPP that propagates along the metal film plane with its electromagnetic field strongly confined to the Au–air interface. The complex propagation constant of this SPP is denoted by $\tilde{\kappa}_{sp} = \kappa'_{sp} + i\kappa''_{sp}$, with its real and imaginary parts representing the SPP's wavenumber and attenuation coefficient, respectively. The SPP is excited in the Kretschmann–Raether configuration [26] by transverse magnetic (TM) polarized light. In this configuration, the incident light impinges onto the Au film from the glass side and couples into the SPP when its wave vector component along the film matches the SPP's wavenumber. This coupling results in a characteristic dip in the TM reflectance curve as a function of the incidence angle, which occurs at incidence angles larger than the critical angle for a glass–air interface. The angle at which the dip reaches its minimum, θ_K, is known as the *Kretschmann angle* and is directly related to the value of κ'_{sp}. On the other hand, the width of the dip is directly related to the value of κ''_{sp}.

The experimental setup is illustrated in Fig. 1. A Ti:sapphire mode-locked oscillator/amplifier system is used to generate nearly transform-limited pulses with a measured pulse duration (full width at half-maximum) of $t_p = 107$ fs, a center wavelength of $\lambda_0 = 795.6$ nm, and a repetition rate of $f_r = 333\ Hz$. The laser beam passes through a half-wave plate followed by a polarizing beam splitter in order to control the power of the incident light on the sample and consequently to control the power of the excited SPP. A 2 mm diameter circular aperture is placed just before the sample to produce a spatially uniform beam. The sample prism rests on a motorized rotation stage with an angular resolution of 0.01°. A second right-angle prism is placed in direct contact with the sample prism in order to direct the reflected light to a power detector. Note that the laser pulses travel approximately 5 mm inside the sample prism before hitting the Au film. The dispersion of such a thickness of

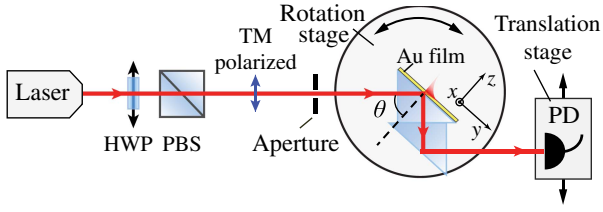

Fig. 1. Experimental setup. HWP, half-wave plate; PBS, polarizing beam splitter; PD, photodetector.

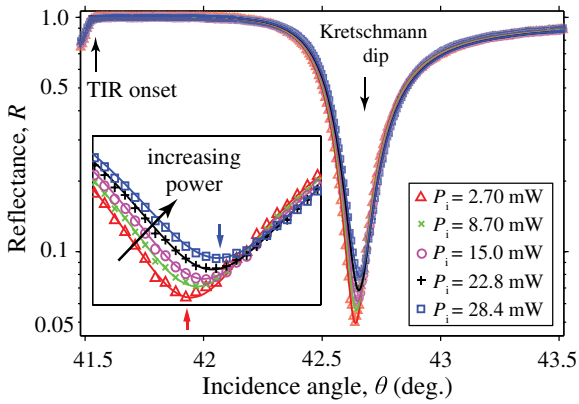

Fig. 2. Reflectance as a function of incidence angle at various incident power levels. The markers are experimental data and the solid lines are numerical fits using Eq. (1). Inset: zoom-in of the Kretschmann dip with the bottom and top arrows indicating Kretschmann angles at low and high power, respectively.

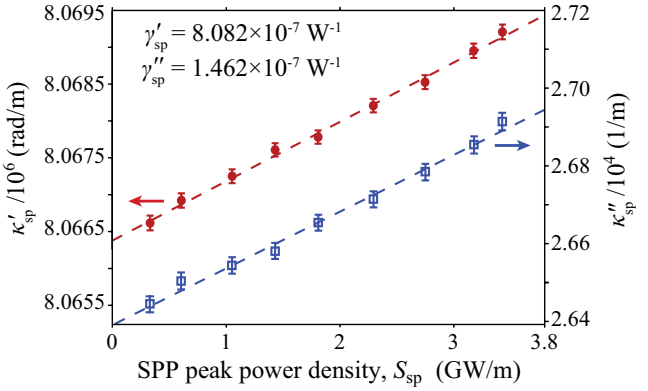

Fig. 3. Real (red filled circles) and imaginary (blue open squares) parts of the SPP propagation constant $\tilde{\kappa}_{sp}$ as a function of effective power density, S_{sp}. The nonlinear parameter $\tilde{\gamma}_{sp}$ is obtained from the slope of the linear fits (dashed lines) to the data.

glass does not introduce significant temporal broadening to the optical pulse.

We measured the TM reflectance as a function of the incidence angle θ at various incident average powers, P_i, ranging from 2.7 to 28.4 mW; five representative curves of these measurements are plotted in Fig. 2. The critical angle that marks the onset of the total internal reflection region is indicated by an arrow. In order to better observe the change in the angular reflectance curve, we show in the inset of Fig. 2 the reflectance over a narrower range of incidence angles. One can see that as P_i increases, θ_K shifts toward a larger angle and the depth of the reflectance dip is reduced. At the same time, although less evident from the figure, the width of the dip increases with the incident power.

In order to quantify the power dependence of $\tilde{\kappa}_{sp}$, we adopt an asymmetric SPP reflectance model [27] with the following expression to fit the experimental data:

$$\mathcal{R}(\theta) \approx \rho_0 \left[1 - \frac{\rho_s + \rho_a \left(2\pi\lambda_0 \sqrt{\varepsilon_g} \sin\theta - \kappa'_{sp} \right)}{\left(2\pi\lambda_0 \sqrt{\varepsilon_g} \sin\theta - \kappa'_{sp} \right)^2 + (\kappa''_{sp})^2} \right], \quad (1)$$

where ρ_0 is a quantity associated with the Fresnel reflection coefficient at the glass–Au interface, ρ_s and ρ_a are quantities that control the symmetry and asymmetry of the reflectance curve, respectively, and ε_g is the relative dielectric permittivity of the glass substrate, which is measured to be 2.2765 through the determination of the critical angle. The fits of Eq. (1) to the experimental data are plotted in solid curves in Fig. 2. For all cases, the R^2 parameter that characterizes the goodness of the fit [28] is larger than 0.998 and the root-mean-squared (RMS) error is smaller than 0.0031.

The effective peak power density carried by the SPP for a given incident average power P_i is estimated through the relation $S_{sp} = (1 - \mathcal{R}) P_i \ell_{sp} / f_r t_p A$, where A is the beam's transverse area projected onto the metal surface and $\ell_{sp} = (2\kappa''_{sp})^{-1}$ is the SPP's effective propagation length. The values of κ'_{sp} and κ''_{sp} as functions of S_{sp} are plotted in Fig. 3 with the dashed lines representing linear fits to the data. There is a clear linear relationship between $\tilde{\kappa}_{sp}$ and S_{sp}, which is indicative of a self-phase modulation, whereby $\tilde{\kappa}_{sp}$ is modified by the power of the SPP itself following the relation

$$\tilde{\kappa}_{sp} = \tilde{\kappa}_{sp,0} + \tilde{\gamma}_{sp} S_{sp}. \quad (2)$$

Here, $\tilde{\kappa}_{sp,0}$ is the propagation constant of the SPP in the linear regime and $\tilde{\gamma}_{sp} = \gamma'_{sp} + i\gamma''_{sp}$ is the complex nonlinear parameter of the SPP, with its real and imaginary parts characterizing the extent of nonlinear phase and nonlinear absorption experienced by the SPP, respectively. Using the data in Fig. 3, we obtain $\tilde{\kappa}_{sp,0} = (806.63 + i2.638) \times 10^4$ m^{-1} from the intersection of the fits with the ordinate and $\tilde{\gamma}_{sp} = (8.08 + i1.46) \times 10^{-7}$ W^{-1} from the slope of the fits. Note that S_{sp} has units of power per unit length (W/m) due to the one-dimensional nature of the SPP, and that $\tilde{\gamma}_{sp}$ has units of inverse power (W^{-1}) rather than the more conventional units of length per unit of power that arise for plane wave propagation in bulk [6].

From the complex nonlinear parameter $\tilde{\gamma}_{sp}$, we can estimate the nonlinear absorption coefficient $\alpha_{NL} = \gamma''_{sp} S_{sp}$ and the nonlinear phase shift $\phi_{NL} = \gamma'_{sp} S_{sp} \ell_{sp}$. Consider the maximum incident power used in the experiment, for which we obtain $\ell_{sp} = 18.53$ μm and $S_{sp} = 3.43$ GW/m. Using the extracted value of γ''_{sp}, we obtain $\alpha_{NL} = 501$ m^{-1}. From this result, it is clear that the effective propagation length of the SPP is not affected significantly by the nonlinear absorption, as the contribution of α_{NL} to the value of κ''_{sp} is only about 2%. On the other hand, using the extracted value of γ'_{sp} we obtain a maximum nonlinear phase shift of $\phi_{NL} = \pi/61$. Note that the magnitude of the achievable nonlinear phase shift under our current configuration is adversely affected by the short propagation length of the SPP. However, one could potentially alleviate this limitation by incorporating optical gain into the SPP waveguide such that ℓ_{sp} is increased significantly [29].

It is worth noting that the heat deposited by individual ultrashort pulses is completely dissipated in a few nanoseconds [30], a period much shorter than the time interval between neighboring pulses in our experiment. Thus, the observed nonlinearity is not the result of heat buildup

in the sample over many light pulses, but rather it takes place within the duration of the laser pulse. The origin of such an ultrafast nonlinearity is believed to be the smearing of the Fermi–Dirac distribution function [5,31] induced by the generation of "hot-electrons" in the conduction band after efficient absorption of SPPs by the metal film.

We shall now turn to our task of extracting the complex value of the third-order nonlinear susceptibility of Au, $\tilde{\chi}^{(3)}_{\mathrm{Au}}$. To achieve this, we developed a nonlinear transfer-matrix (NLTM) model similar in spirit to that formulated by Owens *et al.* [32] to simulate the reflectance curves accounting for the nonlinear response of the materials. The numerical procedure consists of calculating the field distribution throughout the entire structure using a linear transfer-matrix algorithm while accounting for the intensity-dependent permittivity of the Au film in an iterative fashion. For each iteration, the power of an incident plane wave is increased by a small amount and the electromagnetic field in the structure is recalculated by taking the intensity-dependent relative permittivity along the Au film as

$$\tilde{\varepsilon}_{\mathrm{Au}}(z) = \tilde{\varepsilon}_{\mathrm{Au},0} + 3\tilde{\chi}^{(3)}_{\mathrm{Au}}|\mathbf{E}_{\mathrm{Au}}(z)|^2, \tag{3}$$

where we assume that the nonlinear response is solely due to a third-order process. Here, $\tilde{\varepsilon}_{\mathrm{Au},0}$ is the linear relative permittivity of Au, z denotes the position along the direction normal to the film's surface, and $\mathbf{E}_{\mathrm{Au}}(z)$ is the electric field distribution in the Au film calculated in the previous iteration. We ensure good accuracy of the results by resolving the field distribution $\mathbf{E}_{\mathrm{Au}}(z)$ in steps of $\delta z = 0.48$ nm and by incorporating enough iteration steps so that a convergent result is achieved.

Note that our NLTM model assumes an instantaneous response of $\tilde{\chi}^{(3)}_{\mathrm{Au}}$ and a continuous-wave excitation at a single wavelength λ_0. Such an approximation is valid since the wavelength-induced variation of the Kretschmann angle within our pulse bandwidth is negligible and the value of $\tilde{\chi}^{(3)}_{\mathrm{Au}}$ can also be approximated to be constant over the pulse bandwidth [18].

We first determine the value of $\tilde{\varepsilon}_{\mathrm{Au},0}$ by fitting the reflectance curve obtained from the linear transfer-matrix model to a reflection curve predicted by Eq. (1) using the linear propagation constant value of $\tilde{\kappa}_{\mathrm{sp},0} = (806.63 + i2.638) \times 10^4\ \mathrm{m}^{-1}$ extracted from the measurements (cf. Fig. 3). This yields a value of $\tilde{\varepsilon}_{\mathrm{Au},0} = -25.339 + i2.003$, which is in good agreement with the value given in Palik's compendium [33]. We then proceed to fit the NLTM model to all the experimental reflection curves measured at nine different power levels by using $\tilde{\chi}^{(3)}_{\mathrm{Au}}$ as the only fitting parameter. Such a procedure gives $\tilde{\chi}^{(3)}_{\mathrm{Au}} = (4.67 + i3.03) \times 10^{-19}\ \mathrm{m}^2/\mathrm{V}^2$, and the fitted results (solid lines) for reflections at five representative power levels are plotted in Fig. 4. One can see that the fitted results of our numerical model are in good agreement with all the experimental data, and reveal accurately the nonlinear power dependence of the reflection curves. The RMS error for all the fits is small, ranging between 0.018 and 0.026. Note that there is no appreciable difference in the fitting result whether the nonlinear response of the glass and the air is considered or not. This is

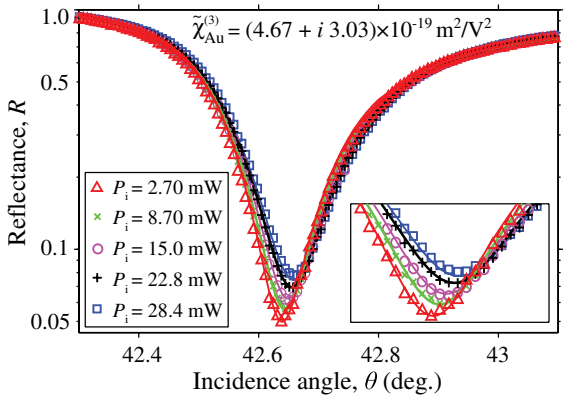

Fig. 4. Measured reflectance as a function of incidence angle at various incident power levels (markers) and numerical fits obtained with the NLTM model using $\tilde{\chi}^{(3)}_{\mathrm{Au}}$ as the only fitting parameter (solid lines). Inset: zoom-in of the Kretschmann dip.

expected since the nonlinear susceptibilities of these media are several orders of magnitude smaller than the value of $\tilde{\chi}^{(3)}_{\mathrm{Au}}$ extracted here [6].

The fact that a single fitting parameter reproduces the reflectance curves at a large range of incident power levels is a strong indication that the extracted value of $\tilde{\chi}^{(3)}_{\mathrm{Au}}$ is accurate. Note that the standard z-scan technique has been used to measure the nonlinear absorption coefficient of Au [34,35]. However, the value of the nonlinear refraction coefficient is often too small and, hence, suffers from poor signal-to-noise ratio in z-scan measurements. For that reason, the nonlinear refraction coefficient is often taken to be zero when converting z-scan results to the value of $\tilde{\chi}^{(3)}$. While such an assumption is reasonable in estimating the magnitude of $\tilde{\chi}^{(3)}$, it could potentially lead to inaccuracies in the value and even the sign of the real part of $\tilde{\chi}^{(3)}$. Thus, the measurement procedure presented here serves as a reliable alternative to measure the complex optical nonlinearity of metallic materials.

With this in mind, we proceed to compare our value of $\tilde{\chi}^{(3)}_{\mathrm{Au}}$ with that estimated from the work of Rotenberg *et al.* [12]. These authors reported measurements of the nonlinear absorption coefficient of a Au film via z-scan using 100 fs laser pulses at $\lambda_0 = 630$ nm. From their results, we find, by taking the nonlinear refraction coefficient to be identically zero, that $\tilde{\chi}^{(3)} \approx (-7.6 + i0.4) \times 10^{-19}\ \mathrm{m}^2/\mathrm{V}^2$. Note that the sign of the real part is reversed relative to our result. Nonetheless, we observe that the magnitudes of both results are of the same order.

In summary, we have studied the nonlinear response of an SPP supported by a Au film in a Kretschmann–Raether configuration bounded by air at $\lambda_0 = 796.5$ nm using laser pulses with a duration of approximately 100 fs. We have observed experimentally the power dependence of the Kretschmann dip in the angular reflectance curve for TM light beyond the critical angle, and have consequently obtained the complex-valued nonlinear parameter that characterizes the extent of nonlinear phase and nonlinear absorption experienced by the SPP. Furthermore, we have developed an NLTM model, which can extract reliably the complex third-order nonlinear susceptibility, $\tilde{\chi}^{(3)}$, of gold from the TM reflectance

curves measured at various power levels. Our procedure provides a robust alternative approach for characterizing the complex-valued $\tilde{\chi}^{(3)}$ of various metallic materials over a broad range of wavelengths.

The work performed at University of Ottawa was supported by the Canada Excellence Research Chairs (CERC) program. This work was supported in part by the US Defense Threat Reduction Agency—Joint Science and Technology Office for Chemical and Biological Defense (grant HDTRA1-10-1-0025). I. D. L. and R. W. B. would like to thank John Sipe and Pierre Berini for useful discussions. Likewise, R. W. B. would like to thank Barry Sanders for useful discussions.

References

1. H. Raether, *Surface Plasmons on Smooth and Rough Surfaces and on Gratings* (Springer, 1988).
2. M. Kauranen and A. V. Zayats, Nat. Photonics **6**, 737 (2012).
3. W. L. Barnes, A. Dereux, and T. W. Ebbesen, Nature **424**, 824 (2003).
4. J. A. Schuller, E. S. Barnard, W. Cai, Y. C. Jun, J. S. White, and M. L. Brongersma, Nat. Mater. **9**, 193 (2010).
5. F. Hache, D. Ricard, C. Flytzanis, and U. Kreibig, Appl. Phys. A **47**, 347 (1988).
6. R. W. Boyd, *Nonlinear Optics*, 3rd ed. (Academic, 2008).
7. M. Breit, V. A. Podolskiy, S. Grésillon, G. von Plessen, J. Feldmann, J. C. Rivoal, P. Gadenne, A. K. Sarychev, and V. M. Shalaev, Phys. Rev. B **64**, 125106 (2001).
8. S. I. Bozhevolnyi, J. Beermann, and V. Coello, Phys. Rev. Lett. **90**, 197403 (2003).
9. J. Renger, R. Quidant, N. van Hulst, and L. Novotny, Phys. Rev. Lett. **104**, 046803 (2010).
10. T. Utikal, T. Zentgraf, T. Paul, C. Rockstuhl, F. Lederer, M. Lippitz, and H. Giessen, Phys. Rev. Lett. **106**, 133901 (2011).
11. I.-Y. Park, S. Kim, J. Choi, D.-H. Lee, Y.-J. Kim, M. F. Kling, M. I. Stockman, and S.-W. Kim, Nat. Photonics **5**, 677 (2011).
12. N. Rotenberg, A. D. Bristow, M. Pfeiffer, M. Betz, and H. M. van Driel, Phys. Rev. B **75**, 155426 (2007).
13. P. Genevet, J.-P. Tetienne, E. Gatzogiannis, R. Blanchard, M. A. Kats, M. O. Scully, and F. Capasso, Nano Lett. **10**, 4880 (2010).
14. N. B. Grosse, J. Heckmann, and U. Woggon, Phys. Rev. Lett. **108**, 136802 (2012).
15. A. R. Davoyan, I. V. Shadrivov, and Y. S. Kivshar, Opt. Express **16**, 21209 (2008).
16. A. Degiron and D. R. Smith, Phys. Rev. A **82**, 033812 (2010).
17. I. De Leon, J. E. Sipe, and R. W. Boyd, Phys. Rev. A **89**, 013855 (2014).
18. A. Marini, M. Conforti, G. D. Valle, H. W. Lee, W. Chang, Tr. X. Tran, M. A. Schmidt, S. Longhi, P. S. J. Russell, and F. Biancalana, New J. Phys. **15**, 013033 (2013).
19. Y. Liu, G. Bartal, D. A. Genov, and X. Zhang, Phys. Rev. Lett. **99**, 153901 (2007).
20. E. Feigenbaum and M. Orenstein, Opt. Lett. **32**, 674 (2007).
21. A. Marini, D. V. Skryabin, and B. Malomed, Opt. Express **19**, 6616 (2011).
22. M. Perner, P. Bost, U. Lemmer, G. von Plessen, J. Feldmann, U. Becker, M. Mennig, M. Schmitt, and H. Schmidt, Phys. Rev. Lett. **78**, 2192 (1997).
23. K. F. MacDonald, Z. L. Samson, M. I. Stockman, and N. I. Zheludev, Nat. Photonics **3**, 55 (2008).
24. G. A. Wurtz, R. Pollard, W. Hendren, G. P. Wiederrecht, D. J. Gosztola, V. A. Podolskiy, and A. V. Zayats, Nat. Nanotechnol. **6**, 107 (2011).
25. S. Toroghi and P. G. Kik, Phys. Rev. B **85**, 045432 (2012).
26. E. Kretschmann, Z. Phys. **241**, 313 (1971).
27. K. Kurihara, K. Nakamura, and K. Suzuki, Sens. Actuators B Chem. **86**, 49 (2002).
28. N. R. Draper and H. Smith, *Applied Regression Analysis* (Wiley, 1998).
29. P. Berini and I. De Leon, Nat. Photonics **6**, 16 (2011).
30. M. van Exter and A. Lagendijk, Phys. Rev. Lett. **60**, 49 (1988).
31. C. K. Sun, F. Vallee, L. H. Acioli, E. P. Ippen, and J. G. Fujimoto, Phys. Rev. B **50**, 15337 (1994).
32. D. T. Owens, C. Fuentes-Hernandez, J. M. Hales, J. W. Perry, and B. Kippelen, Opt. Express **18**, 19101 (2010).
33. E. D. Palik, *Handbook of Optical Constants of Solids* (Academic, 1985).
34. D. D. Smith, Y. Yoon, R. W. Boyd, J. K. Campbell, L. A. Baker, R. M. Crooks, and M. George, J. Appl. Phys. **86**, 6200 (1999).
35. E. Xenogiannopoulou, P. Aloukos, S. Couris, E. Kaminska, A. Piotrowska, and E. Dynowska, Opt. Commun. **275**, 217 (2007).